

MIT Open Access Articles

Methodological Standardization for the Pre-Clinical Evaluation of Renal Sympathetic Denervation

The MIT Faculty has made this article openly available. **Please share** how this access benefits you. Your story matters.

Citation: Sakakura, Kenichi et al. "Methodological Standardization for the Pre-Clinical Evaluation of Renal Sympathetic Denervation." *JACC: Cardiovascular Interventions* 7, 10 (October 2014): 1184–1193 © 2014 American College of Cardiology Foundation

As Published: <http://dx.doi.org/10.1016/J.JCIN.2014.04.024>

Publisher: Elsevier

Persistent URL: <http://hdl.handle.net/1721.1/112781>

Version: Author's final manuscript: final author's manuscript post peer review, without publisher's formatting or copy editing

Terms of use: Creative Commons Attribution-NonCommercial-NoDerivs License





Published in final edited form as:

JACC Cardiovasc Interv. 2014 October ; 7(10): 1184–1193. doi:10.1016/j.jcin.2014.04.024.

Methodological Standardization for the Preclinical Evaluation of Renal Sympathetic Denervation

Kenichi Sakakura, MD, Elena Ladich, MD, Elazer R. Edelman, MD, Peter Markham, James R.L. Stanley, DVM, John Keating, DVM, Frank D. Kolodgie, PhD, Renu Virmani, MD, and Michael Joner, MD

CVPath Institute, Inc. (KS, EL, FDK, RV, MJ), Gaithersburg, MD; CBSET (EE, PM, JS, JK), Lexington, MA

Abstract

Transcatheter ablation of renal autonomic nerves is a viable option for the treatment of resistant arterial hypertension; however, structured preclinical evaluation with standardization of analytical procedures remains a clear gap in this field. Here we discuss the topics relevant to the preclinical model for the evaluation of renal denervation (RDN) devices and report methodologies and criteria towards standardization of the safety and efficacy assessment, including histopathological evaluations of the renal artery, peri-arterial nerves, and associated peri-adventitial tissues. The preclinical swine renal artery model can be used effectively to assess both the safety and efficacy of RDN technologies. Assessment of the efficacy of RDN modalities primarily focuses on the determination of the depth of penetration of treatment-related injury (eg, necrosis) of the peri-arterial tissues and its relationship (ie, location and distance) and affect on the associated renal nerves and the correlation thereof with proxy biomarkers including renal norepinephrine concentrations and nerve-specific immunohistochemical stains (eg, tyrosine hydroxylase). The safety evaluation of RDN technologies involves assessing for adverse effects on tissues local to the site of treatment (ie, on the arterial wall) as well as tissues at a distance (eg, soft tissue, veins, arterial branches, skeletal muscle, adrenal gland, ureters). Increasing experience will help to create a standardized means of examining all arterial beds subject to ablative energy and in doing so enable us to proceed to optimize development and assessment of these emerging technologies.

Introduction

The renal autonomic nervous system plays a major role in the development of arterial hypertension (1). Despite the adoption of contemporary pharmacological treatment, a substantial proportion of patients remain at high risk for subsequent cardio- and cerebrovascular events due to unexplained resistance to drug treatment (2). Renal sympathetic denervation has recently been introduced as a promising option for the

Correspondence: Michael Joner, MD, CVPath Institute, Inc., 19 Firstfield Road, Gaithersburg, MD 20878, TEL: (301) 208-3570, FAX: (301) 208-3745, mjoner@cvpath.org.

Publisher's Disclaimer: This is a PDF file of an unedited manuscript that has been accepted for publication. As a service to our customers we are providing this early version of the manuscript. The manuscript will undergo copyediting, typesetting, and review of the resulting proof before it is published in its final citable form. Please note that during the production process errors may be discovered which could affect the content, and all legal disclaimers that apply to the journal pertain.

treatment of resistant hypertension. Indeed, catheter based radiofrequency (RF) renal denervation has demonstrated effectiveness in clinical studies (3). The increasing prevalence of patients suffering from resistant hypertension on a global scale (2) and the appeal of definitive intervention without life-long obligate adherence to repeated drug dosing has generated fierce demand to refine current catheter-based renal denervation procedures and technologies. To this effect, a variety of technological innovations such as RF and ultrasound catheters, catheter-based micro-infusion of neurotoxic drugs, and externally applied focused ultrasound have been developed, and pre-clinical studies for those devices are ongoing (4). The main objective of these technological endeavors pertains to the effective destruction of peri-arterial sympathetic nerves while preserving arterial morphology and renal function.

In this regard, histopathological assessment of the renal vasculature, along with biomarker analysis of hormones and neurotransmitters, surrounding sympathetic nerves and other regional soft tissue structures is critically important. However, there remains a clear lack of standardization with respect to the histopathological assessment of these tissues following denervation procedures. Most recently, the failure of the first randomized, sham-controlled clinical trial (SYMPPLICITY HTN-3) to reach its primary efficacy endpoint at 6 months underscores the need to revisit existing preclinical animal models (5), since there is no marker of procedural efficacy (ie, confirmation of effective and complete denervation) in humans. In this regard, we aim to establish standardized and reproducible methodology and criteria for histopathological evaluation following renal sympathetic denervation.

Animal model systems

There are a number of means of applying energy to the arterial bed and a number of animal models in which such energies can be applied. The early literature in this field dates back to the ground breaking work of Goldblatt and colleagues who in the 1930's imposed unilateral or bilateral renal arterial constriction to provoke ischemia and release of renin to induce hypertension (6). Their work in dogs defined renal vascular hypertension, helped define the renin-angiotensin-aldosterone system and was followed soon thereafter by a series of experiments demonstrated surgical sympathectomy as possible therapeutic intervention. Other renal injury models emerged including complete ablation or excision of a kidney or infusion of nephrotoxins systemically or locally (7). Other species were considered including small rodents, especially the rat, and occasionally the rabbit (8). As percutaneous technologies have emerged, swine has become a preferred target. Although the bulk of studies are performed in intact animals, it will be increasingly the case that animals with modified renal vasculature and preceding hypertension will be considered. As these models emerge, careful comparison to control states must be attained. Such definition needs to include not only architecture at a defined period of time but the temporal and spatial kinetics of the dynamics and recognition of systemic and circulating effects. These models therefore expand dramatically the tools available to examine ablative technologies but also simultaneously expand the challenges to careful and precise delineate effects. Disease models necessarily disrupt the normal architecture and our view of the normal state is inadequate. Each applied neurotoxic effect is accompanied by idiosyncratic changes and these must be fully defined before we can proceed with understanding how therapeutic

interventions play a role. It will now be especially important as well to track effects over time – we do not know if there is recovery of neural ablation for example. Clinical studies seem to foretell sustained effects but there is not a definitive time when recovery is observed or deemed beyond approach. As disease models are used, these time-dynamic effects will need to be pursued further.

Porcine renovascular anatomy

Although animal models for the assessment of renal sympathetic denervation remain under development, the swine model is the most frequently utilized because of similarity of renovascular anatomy and size to humans (9). Nevertheless, descriptions of porcine perirenal nerve anatomy remain meager. We examined 11 normal renal arteries from 11 pigs to elucidate renovascular anatomy in this species. A total of 6 to 8 sections from each renal artery and surrounding tissues were sectioned at 4 to 5 mm intervals following indelible ink marking of the ventral (orange), dorsal (black), superior (blue) and inferior (green) regions and subjected to routine tissue processing, paraffin embedding, sectioning at 4–5 microns and staining with hematoxylin and eosin (H&E) and Movat pertachrome stains. Digital images were prepared from H&E stained sections at $\times 1.25$ magnification. Images were divided into four quadrants and analyzed using image analysis software (IP Lab for Mac OS X, Scanalytics, Rockville, MD). Length measurements from the luminal surface of the renal artery to the outer nerve contour were performed in each of the four quadrants (ventral, dorsal, superior, and inferior locations). Representative images of distance measurements are shown in Supplemental Figure 1.

Mean length of renal arteries (from aorta to renal artery bifurcation following removal and perfusion fixation by 10% formalin) was 2.1 ± 0.5 cm. A total of 484 nerves from 11 renal arteries were identified from 39 sections (mean number of nerves / section: 12.4 ± 5.7). The mean number of nerves in segments proximal (10.5 ± 6.2), middle (12.0 ± 4.4), and distal (14.0 ± 4.4) to the renal aortic ostium were not significantly different though there was a trend towards greater nerves in the distal versus proximal ($p=0.55$ for proximal vs. middle, $p=0.06$ for proximal vs. distal, $p=0.34$ for middle vs. distal). The mean number of nerves in the ventral location (4.7 ± 2.3) was significantly greater as compared to the dorsal location (2.3 ± 1.1) ($P=0.02$), while there were a similar number of nerves in the superior (3.0 ± 1.8) and inferior arterial locations (2.1 ± 1.2) ($P=0.19$). The cumulative incidence of nerves at distance from lumen is shown in Figure 1. These data are at some odds with Tellez et al. who using renal artery nerve distribution from 5 pigs reported higher nerve density in the proximal segments compared to that in the middle or distal segments (10) Yet, both studies confirmed nerve density in normal swine less than in diseased human (11) and as such if these spatial differences continue to be validated, they will not only influence design of technology but necessitate careful maintenance of specimen alignment and location before affects can be adequately described or compared. Preclinical safety assessment including study of porcine nerve anatomy is important for a standardized evaluation of innovative technology targeted at renal denervation therapy. However, the findings of preclinical studies should be interpreted with caution, as the influence of underlying atherosclerosis in human arteries as well as depth of the nerve distribution may be different and cannot be

assessed in healthy animal models. Moreover, as discussed above further examination of diseased animal model systems will likely soon follow.

Norepinephrine analysis

Researchers have determined that catecholamines such as norepinephrine are important biomarkers that aid in the evaluation of the efficacy of novel therapies in many disease states including neurological disorders, metabolic disease, pain, heart disease, and more specifically drug resistant hypertension. Down-regulation of norepinephrine in renal tissue has been shown to be an indicator of the efficacy of renal denervation therapy in the treatment of drug-resistant hypertension (12,13). The analytical challenges present in the quantitative analysis of norepinephrine in renal tissue are significant. Norepinephrine is present in extremely low endogenous levels, and is subject to extremely rapid metabolic and non-metabolic oxidative degradation. Renal tissue collection techniques must be optimized to avoid autolysis and tissues must be rapidly frozen prior to extraction. Tissue sampling techniques must ensure homogenous sampling as norepinephrine is non-uniformly distributed in the kidney. Studies designed to correlate histopathologic findings to norepinephrine levels must further combine rapid sampling and stabilization of kidney tissue to avoid norepinephrine degradation and perfusion fixation of the arterial and peri-arterial tissue to optimize nerve assessment.

Historical analytical methods of detection of norepinephrine have typically employed high pressure liquid chromatography coupled with electrochemical detection (HPLC-EC) (14). HPLC-EC affords high sensitivity but lacks mass specificity and is therefore subject to potential interferences from a large number of endogenous and exogenous compounds.

The preferred method to quantify norepinephrine in swine renal tissue in the sub-endogenous range best utilizes high throughput tandem mass spectrometry (HPLC-MS/MS) (15). Mass specificity provides the ability to differentiate norepinephrine from epinephrine and other endogenous catecholamines. Methods which employ a stable isotope-labeled analyte (16), Norepinephrine- d_6 , as a surrogate reference standard can leverage the fact that the deuterium labeled norepinephrine and unlabeled norepinephrine behave uniformly during extraction, chromatography, and MS/MS ionization conditions. Extraction and homogenization of norepinephrine from pig kidney tissue must employ a solution that helps enhance the stability of norepinephrine. Through the use of the stable labeled compounds HPLC-MS/MS can be used to determine norepinephrine at greater than two orders of magnitude below endogenous levels. Tissue norepinephrine concentrations in the kidney of the treated arteries are then compared to the tissue norepinephrine concentration in the contralateral untreated kidney, or to a pool of control animals (Supplemental Figure 2) and norepinephrine data are presented as % norepinephrine reduction from control.

Methods of fixation and tissue dissection are described in Supplemental Methods

Macroscopic TTC Staining

It is useful in the early phase of energy-based ablative device development to macroscopically examine the luminal surface of acutely treated renal arteries using 2,3,5-triphenyltetrazolium chloride (TTC) staining. TTC is not a true stain but a water soluble salt that is enzymatically reduced by living cells to a formazan compound which imparts a visibly red coloration (17). TTC staining has been used for decades in research models for the detection and identification of tissue injury/necrosis (e.g., myocardial (18) or cerebral (19) infarction) as non-viable cells lack functional enzymatic processes and do not “stain” but remain pale, in stark contrast to the intensely red coloration of adjacent viable tissue. As such, the exposure of the lumen of acutely treated renal arteries to a TTC solution allows for the precise delineation of the “footprint” of the energy modality and allows one to make macroscopic measurements and correlations with device and histologic parameters.

Histopathologic and Immunohistochemical Stains

Treatment-related soft tissue damage can sometimes be visualized grossly during dissection, however arterial, nerve and soft tissue damages are best visualized on H&E stained sections. Additional stains of elastic fibers, e.g. elastica Van Gieson or Movat pentachrome or Mallory trichrome stains are encouraged as these may provide helpful information with regards to changes in arterial morphology and tissue responses. Immunohistochemical staining for nerve fascicles should be considered in selected sections to evaluate for changes of neurotransmitters or axonal degeneration. Immunostains against S-100 protein (Marker for Schwann and sustentacular cells), neurofilament protein (Marker for neurons and ganglion cells), and glial fibrillary acidic protein (GFAP: Marker for glial cells) are used for the recognition of nerve fascicles (20), whereas stains targeted at tyrosine hydroxylase (TH; which converts tyrosine to DOPA) are used for the presence or absence of norepinephrine synthesis (21). Although DOPA decarboxylase (which converts DOPA to dopamine) is another catecholamine-synthesizing enzyme, immunostaining against DOPA decarboxylase is rarely used in the area of renal denervation because DOPA decarboxylase positive fibers are more sparsely distributed than TH positive fibers in perivascular nerves in the kidney (22). The combination of at least one axonal marker (S-100 protein, neurofilament protein, or GFAP) and a functional marker (TH) may provide meaningful insights into the functional relevance of ablative treatment against resistant hypertension.

Peri-arterial nerves around kidney are comprised of efferent (sympathetic) nerve fibers and afferent (sensory) nerve fibers, and both types of nerves may affect renal sympathetic nerve activity (RSNA) (23). To identify renal afferent nerves, immunostains against calcitonin gene-related peptide (CGRP) and Substance P, which serve as neurotransmitters in sensory nerves (24), have been reported in the literature. However, since immunostaining for CGRP using color-producing reagents has been reported to result in low intensity, the more reliably strong intensity of TH is most often adopted for staining of efferent sympathetic nerve fibers in the immunohistochemical assessment of successful ablation of peri-arterial sympathetic nerves (10). Most importantly, the intensity of color reaction has been shown to be

correlated with presence of viable efferent sympathetic nerve fibers using TH staining (21), an association not found with other immunostain procedures such as CGRP or substance P.

Evaluation

Histologic assessment for nerve fascicles

Treatment related changes to peri-arterial nerves can be assessed using a semi-quantitative ordinal grading system that allows for the assessment of the type of change (ie, degeneration, necrosis, chronic, etc) and its magnitude (eg, minimal, mild, moderate, severe). Figure 2 provides images of a representative grading scheme that refers to effects on both peri- and endoneuronal tissue. The type and magnitude of changes in peri-arterial nerves can represent damages incurred directly with the treatment in the plane of section (ie, nerves that lie directly in the path of treatment) or represent changes associated with injury to the nerve along its length outside the plane of section (ie, upstream or downstream injury). Treatment may affect the perineuronal and/or endoneuronal portions of the renal nerves and present as degenerative, necrotic, or chronic changes. Degenerative changes associated with peri- or endoneuronal injury may include vacuolization and the formation of digestion chambers associated with injury, reversible or irreversible, to the axonal processes of the treated nerve. Necrotic changes may range from pyknosis/karyorrhexis of individual neural nuclei to coagulative necrosis or frank coagulation of the nerve bundle. After resolution of the acute phase of treatment, affected nerves may exhibit a variety of chronic changes including periand endoneurial fibrosis, axonal atrophy or loss. With minimal injury (ie, Grade 1), the nerve would be considered largely intact, and likely functional, but exhibit subtle signs of damage which may include trivial perineuronal inflammation or hemorrhage and limited endoneuronal damage (perineuronal proteoglycan deposition, fibroplasia with little to no vacuolization, pyknosis or increase in cellularity). With mild injury (ie, Grade 2), changes are more conspicuous and/or involving more of the nerve bundle and may include increased cellularity, perineuronal inflammation, fibrosis and/or endoneuronal changes (eg, vacuolization, pyknotic nuclei, or digestion chambers). Nerves with moderate injury (ie, Grade 3) would be interpreted to exhibit more notable changes which may include perineuronal inflammation, fibrosis as well as endoneuronal damage (frequent pyknotic nuclei, digestion chambers, vacuolization, or swelling of endoneuronal tissue). Severe injury (ie, Grade 4) changes are typically overwhelming and may consist of marked perineuronal inflammation and/or fibrosis, and endoneurium damage including effacement of nerve architecture, necrosis, and axonal retraction. Since minimal or mild injury (ie, Grade 2) can be seen even in untreated animals, moderate or severe injury (ie, Grade 3) should be considered to be a definite injury caused by thermal damage or toxins and generally correlates with decreases in renal norepinephrine levels.

Regardless of scoring methodology, the location of all observed nerves should be denoted relative to the area of the treatment (i.e., within or outside the “zone of treatment”) for the purposes of better understanding the treatment efficacy on the total population of nerves available for treatment.

Immunostaining of peri-vascular nerves and scoring criteria

The intensity and distribution of immunostaining can be assessed using a semi-quantitative scoring system (eg, 0= no reaction, 1= patchy/very weak reaction, 2= weak to moderate reaction, 3=strong reaction). Representative images of immunostaining are shown in Figure 3. Typically, a weak reaction (ie, Grade 2), or absence of TH, represents a strong treatment effect as the absence of staining is an indirect sign of functional nerve degeneration and can be correlated with the renal norepinephrine levels. With respect to the functional assessment of nerve viability using immunostaining, the choice of time-point is crucial as immunohistochemical analysis represents a snapshot assessment in the time course of axonal degeneration following renal denervation procedures. If the nerves being examined are less than 7 days of denervation, immunostaining is usually positive despite extensive necrosis, therefore it is not recommended that immunostaining be performed prior to 7 days following denervation procedure.

Histologic assessment of renovascular morphology

Renovascular damage includes endothelial cell loss, thrombus formation and medial damage, which can be assessed along the depth and circumference of the artery. These changes can be assessed using a semi-quantitative ordinal grading system (eg, 0=none, 1=minimal, 2=mild, 3=moderate, and 4=severe). Figure 4 provides representative images of a grading scheme that refers to both endothelial cell loss and medial wall damage. Endothelial loss should be evaluated by the percentage of circumferential endothelial cell loss (Figure 4). Endothelial cell loss is typically observed acutely after treatment and is rarely observed at 28-days. A common characteristic of thermal media injury is smooth muscle cell (SMC) loss/necrosis with proteoglycan and/or fibrous tissue replacement. The depth of media damage is evaluated by the percentage of smooth muscle cell loss in relation to media thickness (Figure 4). When evaluating the depth of medial damage, the presence of media thinning should be reported. Media thinning is defined as thickness of the media at the site of damage (mm)/unaffected media thickness (mm) with < 0.5 representing severe smooth muscle cell loss/necrosis within the media. In addition, the cross-sectional dimension of medial damage can be assessed as circumferential loss/necrosis of SMCs. When evaluating media damage, it is recommended to use the Movat pentachrome stain as proteoglycan deposition can be easily appreciated.

Histologic assessment for peri-arterial tissues and organs

Peri-arterial tissues such as fat, collagen, renal veins, arterioles, ureters, adrenal glands, skeletal muscle, viscera, and the kidney should all be systematically evaluated for signs of injury. Again, a semi-quantitative ordinal grading system (eg., 0=none, 1=minimal, 2=mild, 3=moderate, and 4=severe) can be utilized to score observed changes. It is important to mention that the risk of thermal renal vein injury and thrombosis is far less than that of thermal arterial injury. Also, most venous injuries initiate at the abluminal surface, whereas most of arterial injuries begins at the luminal surface, of course depending upon the mode of denervation used. However, as the veins are thin it is important to appropriately assess the venous injury and/or thrombosis. Arteriolar damage usually correlates with the overall nerve damage. Typical severe (grade 4) injury of arterioles is fibrinoid necrosis, which is most

often observed acutely but often persists up to 28-days. A representative scoring criteria for arterioles damages is shown in Supplemental Figure 3. Injury to the ureters is evaluated by the extent of edema and necrosis (submucosal, muscular, and periureteral surrounding tissue) as well as mucosal ulceration. However, ureter injury is not frequent, because the remote anatomical position of the ureter relative to the ablation site precludes it from direct thermal injury. As a direct sign of thermal injury on collagen/adipose tissue, the presence of denatured collagen should be assessed, which can easily be detected by elastica stains. Similarly periadventitial fat may undergo necrosis with saponification and surrounding acute inflammation followed by chronic inflammation (25,26). This usually appears as shadowy outline of adipose cells with saponification. Representative scoring criteria for fat damages are shown in Supplemental Figure 4.

Not only are direct renal and soft tissue important but attention should be also directed towards lymph node damage, skeletal muscle and adjoining viscera (e.g., the cecum and adrenal glands). Therefore these structures should be routinely assessed by the individual necropsy prosector and submitted for histologic assessment for the extent and type of damage if present.

Advantage of the combination of various stains

The combination of an elastica stain with a standard H&E stain will more reliably allow the appropriate assessment of nerve injury, arterial wall injury, and soft tissue injury (Supplemental Figure 5) as the information of both staining protocols is cumulative. For example, proteoglycan replacement (green tissue) within the arterial media can easily be recognized by a Movat pentachrome stain. Denatured collagen is clearly distinguished as black tissue by Movat pentachrome stain whereas H&E gives a blue tinge of staining and may be difficult to identify. Also, perineural fibrosis can easily be recognized by Movat pentachrome stain. Therefore, we recommend using this stain as well as H&E stain routinely for the evaluation of arterial, soft tissue, and nerve injuries.

Quadrant analysis and deepest soft tissue damage

To capture the entire spectrum of thermal and/or toxic tissue damage along the vascular circumference a cross-sectional quadrant analysis is recommended as shown in Supplemental Figure 6 where one quadrant refers to <25% circumferential area, 2 quadrants 26–50% circumferential area, 3 quadrants 51–75% circumferential area, and 4 quadrants refer to >75% circumferential area. Obtaining the number of quadrants with injured nerve fascicles relative to quadrants with the presence of nerve fascicles enables the capturing of differences in circumferential thermal injury among different devices. The distance from renal arterial lumen to deepest tissue damage (nerves, vein, arterioles, or other soft tissues) determines the effective depth of thermal and/or toxic injury among different devices. Figure 5 shows representative images of distance measurements. Combining the information retrieved from cross-sectional quadrant analysis and penetration of the depth of thermal injury provides unique information regarding the number of quadrants affected and the adequacy of the denervated area in relation to circumferential discontinuity of innervation of the kidney.

Summary

Summary of methodological standard for the preclinical evaluation of RDN is shown in Table 1. The purpose of this document is to guide and standardize the preclinical histopathological assessment with regards to renal sympathetic denervation procedures. Standardization of histopathological assessment remains an unmet need in this field, which may ultimately facilitate understanding of underlying mechanisms after renal denervation and further to help assess which device is the more appropriate and what advantages each device may offer from the currently available technologies. As research in this area evolves, updates will be mandatory to warrant appropriate adoption into clinical practice.

Supplementary Material

Refer to Web version on PubMed Central for supplementary material.

Acknowledgement

CVPPath Institute Inc., Gaithersburg, Maryland, USA provided full support for works of KS, EL, FK, RV and MJ. ERE was supported by grants from NIH including R01 GM49039, and PM, JK and JS were supported by CBSET, Lexington MA. Dr. Sakakura is supported by a research fellowship from the Banyu Life Science Foundation International. This manuscript would not have been possible without the support of the following companies: Biosense Webster (Irwin dale, CA, USA), Medtronic (Minneapolis, MN, USA), Kona Medical (Bellevue, WA, USA), and ReCor Medical (Menlo Park, CA, USA).

Disclosures: Dr. Sakakura has received speaking honorarium from Abbott Vascular, Boston Scientific, and Medtronic CardioVascular. Dr. Virmani receives research support from 480 Biomedical, Abbott Vascular, Atrium, Biosensors International, Biotronik, Boston Scientific, Cordis J&J, GSK, Kona, Medtronic, Microport Medical, OrbusNeich Medical, ReCor, SINO Medical Technology, Terumo Corporation, and W.L. Gore. ; has speaking engagements with Merck; receives honoraria from 480 Biomedical, Abbott Vascular, Biosense Webster, Biosensors International, Boston Scientific, Claret Medical, CeloNova, Cordis J&J, Lutonix, Medtronic, Terumo Corporation, and W.L.Gore; and is a consultant for 480 Biomedical, Abbott Vascular, Medtronic, and W.L. Gore. Dr. Joner is a consultant for Biotronik and Cardionovum, and has received speaking honorarium from Abbott Vascular, Biotronik, Medtronic, and St. Jude.

Abbreviations

RDN	renal denervation
RF	radiofrequency
HPLC-EC	high pressure liquid chromatography coupled with electrochemical detection
HPLC-MS/MS	high throughput tandem mass spectrometry
TTC staining	2,3,5-triphenyltetrazolium chloride (TTC) staining
GFAP	glial fibrillary acidic protein
TH	tyrosine hydroxylase
CGRP	calcitonin gene-related peptide
RSNA	renal sympathetic nerve activity
SMC	smooth muscle cell

References

1. DiBona GF. Sympathetic nervous system and hypertension. *Hypertension*. 2013; 61:556–560. [PubMed: 23357181]
2. Calhoun DA, Jones D, Textor S, et al. Resistant hypertension: diagnosis, evaluation, and treatment. A scientific statement from the American Heart Association Professional Education Committee of the Council for High Blood Pressure Research. *Hypertension*. 2008; 51:1403–1419. [PubMed: 18391085]
3. Esler MD, Krum H, Sobotka PA, Schlaich MP, Schmieder RE, Bohm M. Renal sympathetic denervation in patients with treatment-resistant hypertension (The Symplicity HTN-2 Trial): a randomised controlled trial. *Lancet*. 2010; 376:1903–1909. [PubMed: 21093036]
4. Compiled by Rocha-singh K. Renal artery denervation: A Brave New Frontier. *Endovascular Today*. 2012 Feb.:45–53.
5. Bhatt DL, Kandzari DE, O'Neill WW, et al. A Controlled Trial of Renal Denervation for Resistant Hypertension. *N Engl J Med*. 2014
6. Berman LB. The Goldblatt kidney. *Arch Intern Med*. 1971; 128:306–308. [PubMed: 5564212]
7. Katz MA, Shear L. Effects of renal nerves on renal hemodynamics. II. Renal denervation models. *Nephron*. 1975; 14:390–397. [PubMed: 1134615]
8. Bello-Reuss E, Colindres RE, Pastoriza-Munoz E, Mueller RA, Gottschalk CW. Effects of acute unilateral renal denervation in the rat. *J Clin Invest*. 1975; 56:208–217. [PubMed: 1141432]
9. Rippey MK, Zarins D, Barman NC, Wu A, Duncan KL, Zarins CK. Catheter-based renal sympathetic denervation: chronic preclinical evidence for renal artery safety. *Clin Res Cardiol*. 2011; 100:1095–1101. [PubMed: 21796327]
10. Tellez A, Rousselle S, Palmieri T, et al. Renal artery nerve distribution and density in the porcine model: biologic implications for the development of radiofrequency ablation therapies. *Transl Res*. 2013; 162:381–389. [PubMed: 23911638]
11. Atherton DS, Deep NL, Mendelsohn FO. Micro-anatomy of the renal sympathetic nervous system: a human postmortem histologic study. *Clin Anat*. 2012; 25:628–633. [PubMed: 21976355]
12. Krum H, Schlaich M, Whitbourn R, et al. Catheter-based renal sympathetic denervation for resistant hypertension: a multicentre safety and proof-of-principle cohort study. *Lancet*. 2009; 373:1275–1281. [PubMed: 19332353]
13. Esler M, Jennings G, Korner P, et al. Assessment of human sympathetic nervous system activity from measurements of norepinephrine turnover. *Hypertension*. 1988; 11:3–20. [PubMed: 2828236]
14. Tsunoda M. Recent advances in methods for the analysis of catecholamines and their metabolites. *Anal Bioanal Chem*. 2006; 386:506–514. [PubMed: 16924378]
15. Taylor RL, Singh RJ. Validation of liquid chromatography-tandem mass spectrometry method for analysis of urinary conjugated metanephrine and normetanephrine for screening of pheochromocytoma. *Clin Chem*. 2002; 48:533–539. [PubMed: 11861444]
16. Ji C, Walton J, Su Y, Tella M. Simultaneous determination of plasma epinephrine and norepinephrine using an integrated strategy of a fully automated protein precipitation technique, reductive ethylation labeling and UPLC-MS/MS. *Anal Chim Acta*. 2010; 670:84–91. [PubMed: 20685421]
17. H . The Chemistry of Formazans and Tetrazolium Salts. *Hacettepe Journal of Biology and Chemistry*. 2012; 40:293–301.
18. Bohl S, Medway DJ, Schulz-Menger J, Schneider JE, Neubauer S, Lygate CA. Refined approach for quantification of in vivo ischemia-reperfusion injury in the mouse heart. *Am J Physiol Heart Circ Physiol*. 2009; 297:H2054–H2058. [PubMed: 19820193]
19. Bederson JB, Pitts LH, Germano SM, Nishimura MC, Davis RL, Bartkowski HM. Evaluation of 2,3,5-triphenyltetrazolium chloride as a stain for detection and quantification of experimental cerebral infarction in rats. *Stroke*. 1986; 17:1304–1308. [PubMed: 2433817]
20. Pace V, Perentes E, Germann PG. Pheochromocytomas and ganglioneuromas in the aging rats: morphological and immunohistochemical characterization. *Toxicol Pathol*. 2002; 30:492–500. [PubMed: 12187940]

21. Burgi K, Cavalleri MT, Alves AS, Britto LR, Antunes VR, Michelini LC. Tyrosine hydroxylase immunoreactivity as indicator of sympathetic activity: simultaneous evaluation in different tissues of hypertensive rats. *Am J Physiol Regul Integr Comp Physiol.* 2011; 300:R264–R271. [PubMed: 21148479]
22. Harris T, Muller B, Cotton RG, Borri Voltattorni C, Bell C. Dopaminergic and noradrenergic sympathetic nerves of the dog have different DOPA decarboxylase activities. *Neurosci Lett.* 1986; 65:155–160. [PubMed: 2872622]
23. DiBona GF, Esler M. Translational medicine: the antihypertensive effect of renal denervation. *Am J Physiol Regul Integr Comp Physiol.* 2010; 298:R245–R253. [PubMed: 19955493]
24. Liu L, Barajas L. The rat renal nerves during development. *Anat Embryol (Berl).* 1993; 188:345–361. [PubMed: 7506501]
25. Franco W, Kothare A, Ronan SJ, Grekin RC, McCalmont TH. Hyperthermic injury to adipocyte cells by selective heating of subcutaneous fat with a novel radiofrequency device: feasibility studies. *Lasers Surg Med.* 2010; 42:361–370. [PubMed: 20583242]
26. Smith GW, Rotstein DS, Brownie CF. Abdominal fat necrosis in a pygmy goat associated with fescue toxicosis. *J Vet Diagn Invest.* 2004; 16:356–359. [PubMed: 15305753]

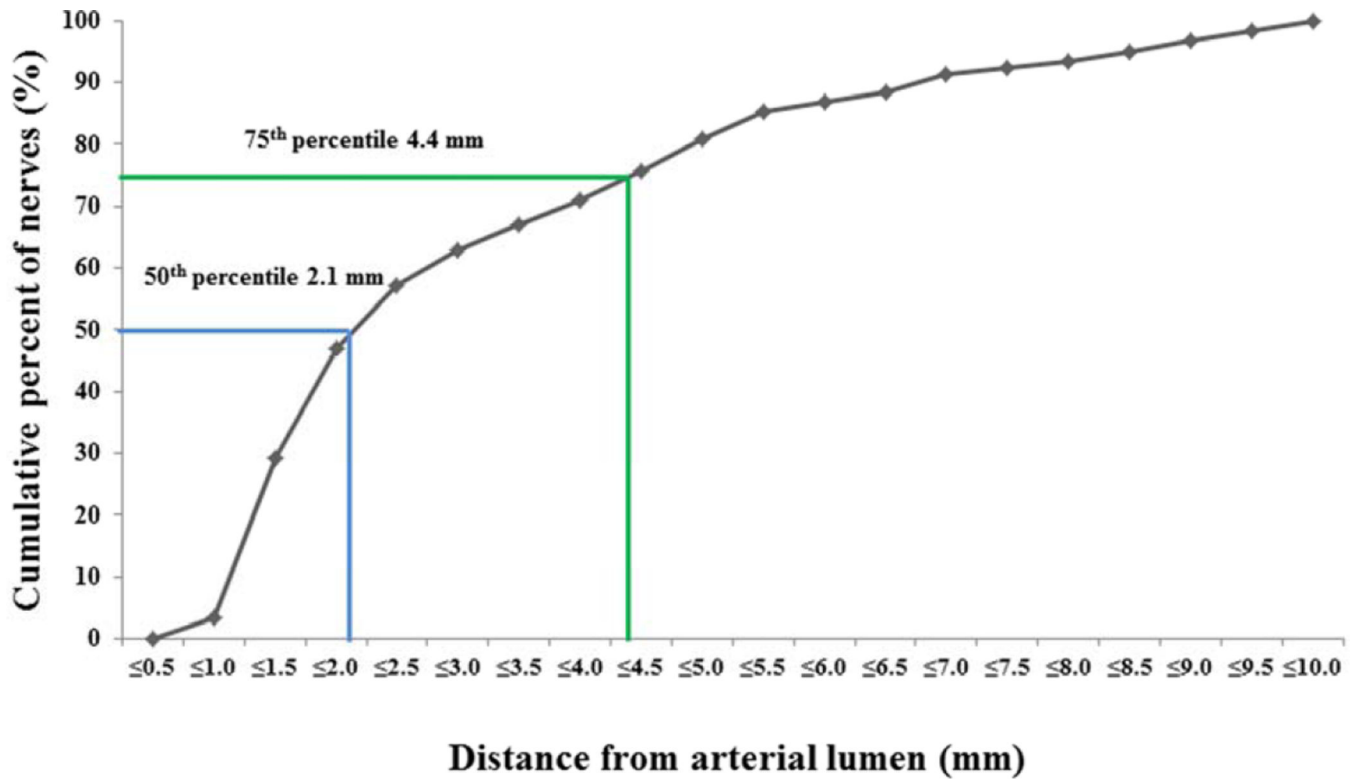


Figure 1. Cumulative incidence of normal perirenal nerve distances from renal arterial lumen
 The cumulative incidence of nerve distance from lumen is calculated from 484 nerves. The 50th percentile of the distance from the arterial lumen to nerve was 2.1mm, whereas 75th percentile in that was 4.4 mm.

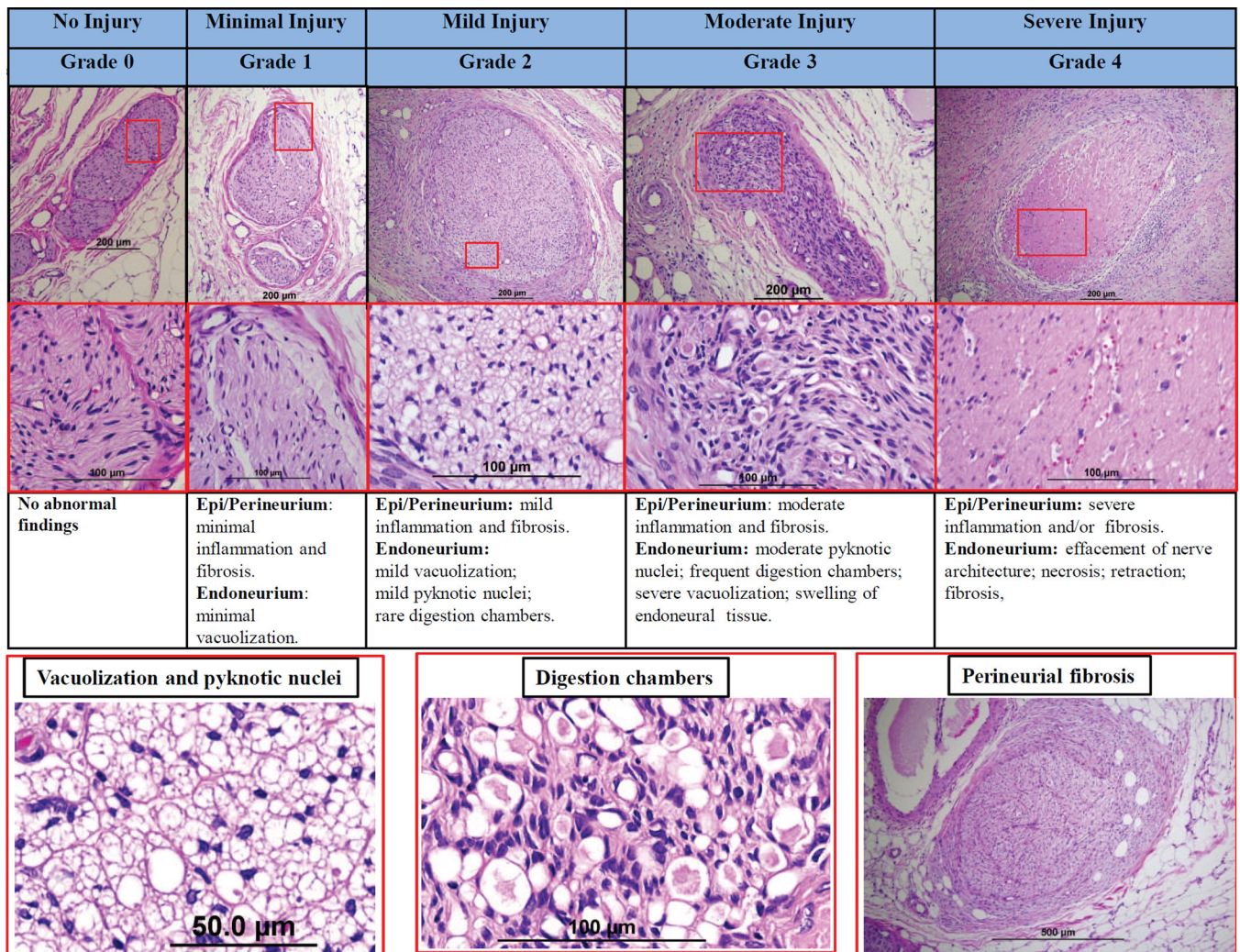


Figure 2. Semi-quantitative grading scheme for nerve changes

Upper panel shows representative images of nerves by increasing grade of injury. Middle panels shows high power images of injured nerves (red boxed area in upper panels) in each grade. Lower panels shows representative images of vacuolization, pyknotic nuclei, digestion chambers, and perineurial fibrosis. All image panels are stained with H&E stain.

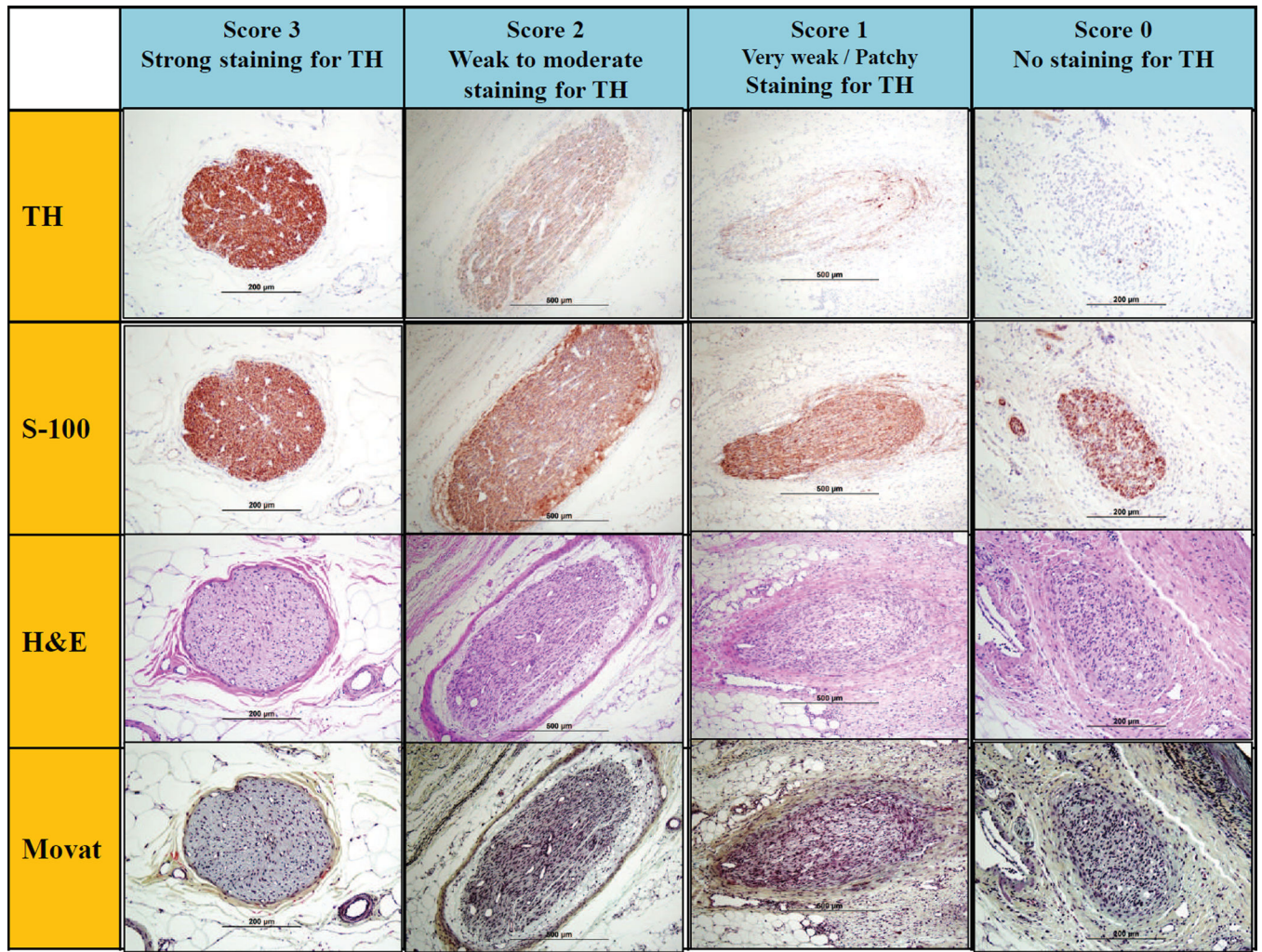


Figure 3. Semi-quantitative scoring criteria for immunostain against tyrosine hydroxylase
 Upper panels are representative images of injured nerves stained by anti-tyrosine hydroxylase (TH) enzyme. Lower panels are corresponding images of injured nerves with H&E and Movat pentachrome stains.

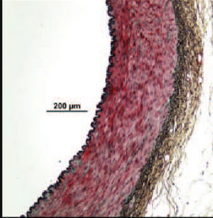
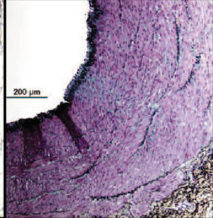
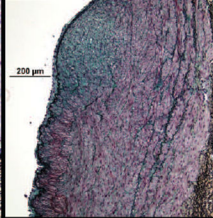
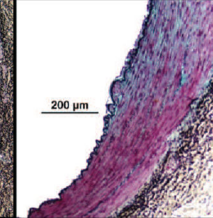
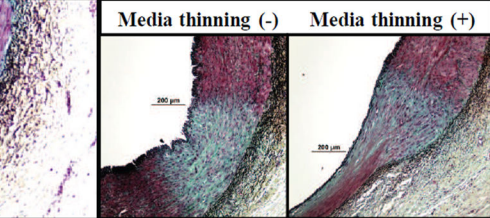
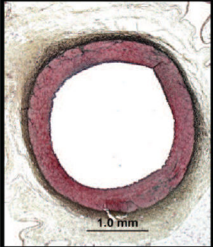
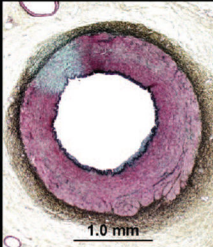
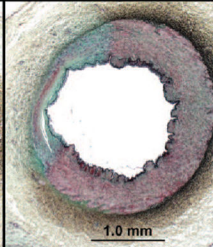
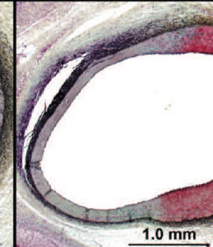
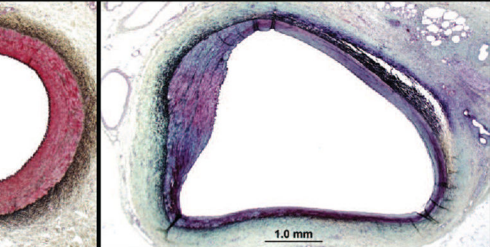
Injury Absent	Minimal Injury	Mild Injury	Moderate Injury	Severe Injury
Grade 0	Grade 1	Grade 2	Grade 3	Grade 4
Endothelial loss 0 % of vessel circumference	Endothelial loss <25 % of vessel circumference	Endothelial loss 25-<50 % of vessel circumference	Endothelial loss 50-<75 % of vessel circumference	Endothelial loss ≥75% of vessel circumference
Medial change Depth 0% of media thickness	Medial change Depth <25 % of media thickness	Medial change Depth 25-<50 % of media thickness	Medial change Depth 50-<75 % of media thickness	Medial change Depth ≥75% of media thickness. Media thinning : Injured media thickness <50% of unaffected media.
				
Medial change Circumferential 0% of vessel circumference	Medial change Circumferential <25 % of vessel circumference	Medial change Circumferential 25-<50 % of vessel circumference	Medial change Circumferential 50-<75 % of vessel circumference	Medial change Circumferential ≥75% of vessel circumference
				

Figure 4. Semi-quantitative grading scheme for renal artery damage

Upper panels represent depth of medial wall injury by the grade of damage, whereas lower panels represent circumferential grade of damage of the medial wall. Note, media thinning can only occur with grade 4 depth of injury and should be distinguished. All images are stained with Movat pentachrome.

Distance from Arterial Lumen to Various Types of Injured Tissue

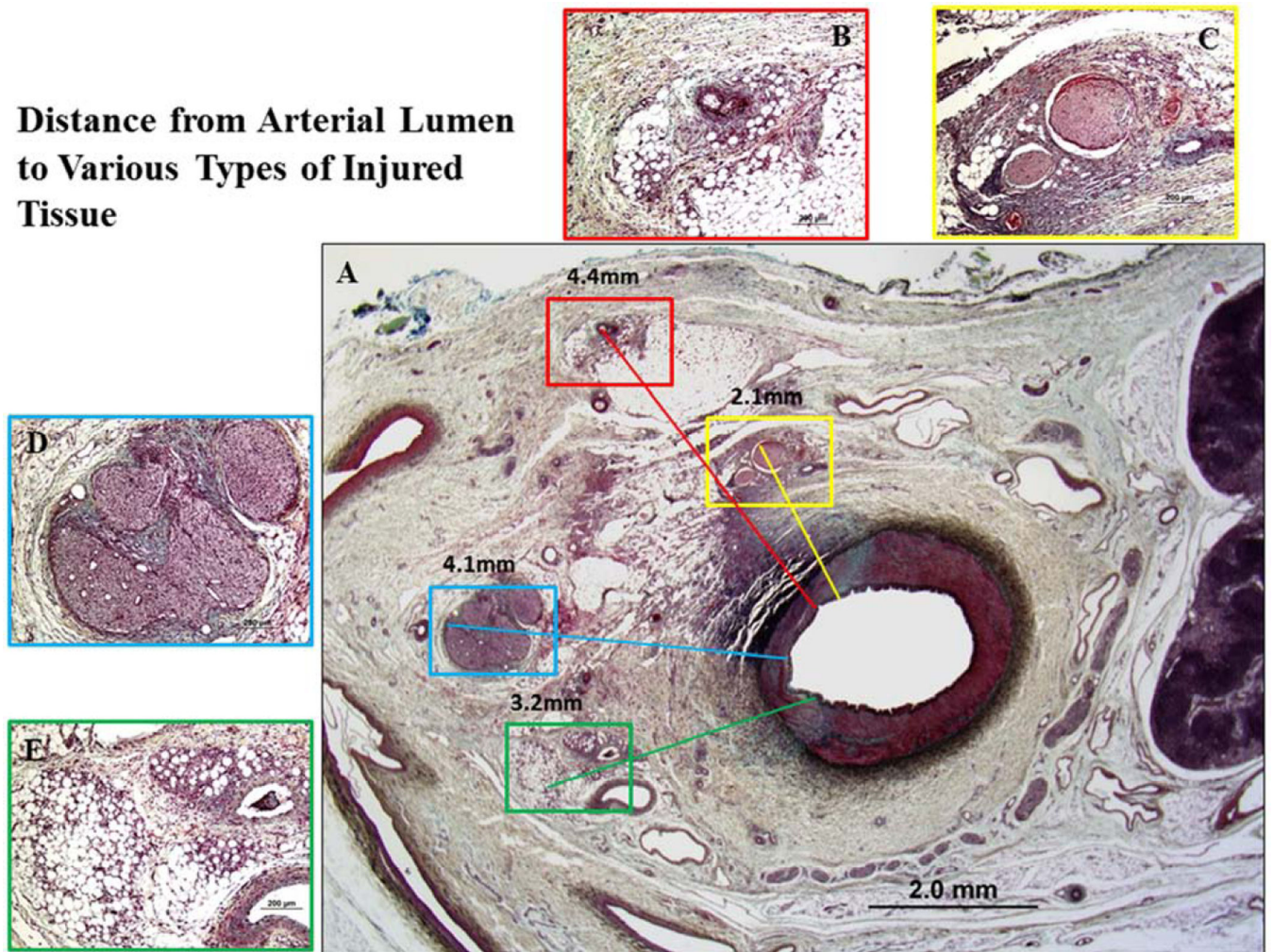


Figure 5. Representative images of distance from arterial lumen to various types of injury
A: Low-power image of a treated renal artery and surrounding perirenal area. **B:** High-power images of injured arterioles (red boxed area in A). The distance from lumen to injured arterioles was 4.4 mm. **C:** High-power image of nerve injury (yellow boxed area in A). The distance from lumen to injured nerves was 2.1 mm. **D:** High-power image of injured nerves (blue boxed area in A). The distance from lumen to injured nerve was 4.1 mm. **E:** High-power image of soft tissue injury (green boxed area in A). The distance from lumen to injured tissue was 3.2 mm.

Table 1

Summary of methodological standard for the Preclinical Evaluation of Renal Sympathetic Denervation.

Category	Methods	Purpose
Biomarker	Kidney norepinephrine levels (HPLC-MS/MS)	Evaluation of the extent of renal sympathetic denervation
Macroscopic evaluation	TTC staining of renal artery	To assess the extent of arterial wall injury
Standard Light Microscopy and morphometry	Semi-quantitative scoring of pathologic changes (grade 0 to grade 4): Nerve, renal artery, vein, arterioles, fat and collagen.	To determine the extent of nerve injury, arterial and surrounding soft tissue injury
	Quadrant analysis (0 to 4 quadrants) for nerve injury and soft tissue injury	Evaluation of circumferential extent of injury
	Depth of tissue injury (mm)	Evaluation of therapeutic penetration
Immunohistochemistry	Semi-quantitative scoring of intensity of immunostaining (score 0 to score 3) by anti-tyrosine hydroxylase	Evaluation of the ability of the nerves to generate nor-epinephrine (functional nerve injury)

Author Manuscript

Author Manuscript

Author Manuscript

Author Manuscript